A comparative study of the osteogenic performance between the hierarchical micro/submicro-textured 3D-printed Ti6Al4V surface and the SLA surface

Jinkai Zhang[a,1], Jiaqiang Liu[b,1], Chengtao Wang[c], Fengshan Chen[a,**], Xudong Wang[b,***], Kaili Lin[b,*]

[a] Department of Orthodontics, School & Hospital of Stomatology, Tongji University; Shanghai Engineering Research Center of Tooth Restoration and Regeneration, Shanghai, 200072, China
[b] Department of Oral & Cranio-Maxillofacial Surgery, Shanghai Ninth People's Hospital, College of Stomatology, Shanghai Jiao Tong University School of Medicine; National Clinical Research Center for Oral Diseases; Shanghai Key Laboratory of Stomatology & Shanghai Research Institute of Stomatology, Shanghai, 200011, China
[c] School of Mechanical Engineering, Shanghai Jiao Tong University, Shanghai, 200240, China

ARTICLE INFO

ABSTRACT

Three-dimensional (3D) printed titanium and its alloys have broad application prospect in the field of biomedical implant materials, although the biological performance of the original surface should be improved. Learning from the development experience of conventional titanium implants, to construct a hierarchical hybrid topological surface is the future direction of efforts. Since the original 3D-printed (3D hereafter) Ti6Al4V surface inherently has micron-scale features, in the present study, we introduced submicron-scale pits on the original surface by acid etching to obtain a hierarchical micro/submicro-textured surface. The characteristic and biological performance of the 3D-printed and acid-etched (3DA hereafter) surface were evaluated *in vitro* and *in vivo,* compared with the conventional sandblasted, large-grit, acid-etched (SLA hereafter) surface. Our results suggested the adhesion, proliferation and osteogenic differentiation of bone marrow derived mesenchymal stromal cells (BMSCs), as well as the *in vivo* osseointegration on 3DA surfaces were significantly improved. However, the overall osteogenic performance of the 3DA surface was not as good as the conventional SLA surface.

1. Introduction

3D printing, an additive manufacturing (AM) process, has gradually evolved as one of the most vital advanced manufacturing technologies due to its inherent advantages, such as high manufacturing efficiency, high utilization ratio of materials and capacity of producing complex structures (e.g. porous scaffolds) [1–4]. Moreover, the most profound advantage of 3D printing is its powerful ability of personalized design and manufacture, which can just meet the demand of precision medicine [5,6]. Actually, some 3D-printed products have already been introduced into clinical application [7]. Our previous research suggested that 3D-printed Ti6Al4V surfaces could promote osteogenic differentiation and early *in vivo* osseointegration after 3 weeks of

implantation compared with conventional machined surfaces [8]. While with the increase of implantation period to 6 weeks, the difference of *in vivo* osseointegration diminished. Therefore, the osteogenic performance of the original 3D-printed surface must be further improved.

Titanium and its alloys have been used as biomedical implant materials for over half of a century and numerous researchers have developed many surface modification methods to improve the biological performance of titanium implants [9–13]. Briefly, biochemical and/or biophysical signals are introduced onto implant surfaces through mechanical, physical or chemical methods, and thus the biological performance is improved [14–16]. Among these strategies, topographical modification has attracted much efforts and is considered as a basic and

stable method [17]. Considering that natural bone consists of hierarchical hybrid structures, from nanoscale to macroscale [18,19], hierarchically textured surface may promote osteogenesis-related functions of osteogenic cells. This hypothesis has been proved by many researches and the most representative hierarchical titanium surface is the SLA surface, which consists of micron-scale (20–40 μm) concaves produced by large-grit sandblasting and submicron-scale (0.5–3 μm) pits produced by acid etching. It has been well revealed that the SLA surface can apparently promote osseointegration and achieve satisfied clinical results [20,21].

Coincidently, 3D-printed Ti6Al4V surfaces inherently present micron-scale topographies, the size of which are at the similar level of large-grit sand-blasted features [8]. Thus, in this study, we employed acid etching to create submicron-scale pits on the original 3D surface, obtaining a hierarchical micro/submicro-textured surface. Meanwhile, the acid etching could serve as a postprocessing procedure to remove the unmelted or weakly connected particles. To control variable and rigorously investigate the effect of surface modification, we kept the original 3D surface as the controlling sample since other postprocessing procedures would definitely alter the original topography. Moreover, we employed the SLA surface as a positive control, to evaluate the biological performance of hierarchically modified 3D-printed Ti6Al4V surfaces.

2. Materials and methods

2.1. Preparation of samples

3D samples were printed by an EOS laser printing system (EOS GmbH Munchen, Germany). Briefly, Ti6Al4V alloy powders (particle size ranging from 20 to 50 μm in diameter) were used as the raw material and experimental samples were fabricated layer by layer. The process was based on selective laser melting technology and the thickness of each single layer was approximately 30 μm. Square discs (10 mm × 10 mm × 2 mm) were prepared for *in vitro* experiments and cylinders (φ 2 mm × 3 mm) were prepared for the *in vivo* test. After thoroughly cleaning, 3D samples were etched in a boiling acid bath consisting of sulfuric acid and hydrochloric acid for 2 min to produce 3DA samples [22]. On the other hand, conventional machined samples were processed by large-grit sandblasting and then etched by the same procedure as 3DA samples to produce SLA samples. All samples were ultrasonically cleaned in acetone, ethanol and distilled water sequentially for 15 min and then steam autoclaved.

2.2. Surface characteristics

The surface morphology of three groups was observed by a scanning electron microscopy (SEM, Hitachi, Japan). Surface roughness parameters were detected by a confocal laser scanning microscope (Olympus, Japan) and three samples for each group were evaluated. Furthermore, the water contact angle of surfaces was measured by an Optical Contact Angle and Tension Meter (SOLON TECH, China).

2.3. In vitro studies

2.3.1. Cell culture

BMSCs were isolated from the femora and tibiae of two-week-old Sprague Dawley (SD) rats. The animal experiments were approved by the Institutional Animal Care and Use Committee of Tongji University. Briefly, bone marrow contents were flushed by alpha-modified Eagle's medium (α-MEM,Hyclone, USA) supplemented with 10% fetal bovine serum (Hyclone, USA) and 1% penicillin/streptomycin (Hyclone, USA) into a 6-cm cell culture dish. Cells were incubated at 37 °C, 5% CO_2 atmosphere and 100% humidity. Medium was replaced every two days, and the 3rd to 5th passages of BMSCs were used in subsequent studies.

2.3.2. Cell morphology

The morphology of adhered cells on 3D, 3DA and SLA surfaces was observed by SEM. BMSCs were seeded on samples at a density of 5×10^4/well and cultured for 24 h. Then the medium containing unattached cells was removed and samples were rinsed gently by phosphate buffer solution (PBS, Hyclone, USA) for three times. Samples were fixed in 2.5% glutaraldehyde for 1 h and rinsed in PBS for three times. Before the SEM scanning, samples were dehydrated in graded ethanol series (35%, 50%, 75%, 90%, 100% twice, each for 10 min) sequentially and freezing dried.

2.3.3. Cell proliferation

Cell proliferation was evaluated by Cell Counting Kit-8 (CCK-8, Beyotime, China). Briefly, BMSCs were seeded on samples in 24-well plates at a density of 1×10^4/well and cultured for 1, 4, 7 and 10 days, respectively. Medium was changed every 2 days. At each timepoint, samples were transferred into new wells and rinsed by PBS and then incubated in 500 μL CCK-8 working solution for 3 h. Finally, 100 μL solution for each sample was transferred into a 96-well plate to detect the absorbance at 450 nm wavelength.

2.3.4. Alkaline phosphatase (ALP) activity assay

Cells were seeded at a density of 2×10^4/well and when cells cultured on tissue culture plates reached 80% confluency, osteogenic inducing initiated. After 4, 7 and 10 days of inducing, samples were transferred to new wells and rinsed with PBS. Then cells on the samples were lysed in 200 μL 0.1% Triton x-100 buffer (Beyotime, China) for 30 min on ice and the lysate was collected into 1.5 mL microcentrifuge tubes. The supernatant was used to detect the ALP activity by an Alkaline Phosphatase Assay Kit (Nan-Jing-Jian-Cheng, China) and total protein concentration was detected by a BCA protein assay kit (Beyotime, China) according to manufacturer's instructions. The ALP activity was calculated and calibrated by the total protein concentration (U/g protein).

2.3.5. Alizarin red staining

After osteogenic inducing (the same procedure as the ALP activity assay) for 14 days, Alizarin red staining was performed to evaluate the mineralization level on the three kinds of surfaces. Briefly, samples were fixed in 4% paraformaldehyde for 30 min and rinsed in PBS before stained in Alizarin red staining solution (Cyagen Biosciences, China) for 15 min. After thoroughly rinsed in distilled water, images of samples were captured by a stereomicroscope (Leica, Germany). Finally, for semiquantitative analysis, the mineralization was eluted in 1 mL 10% hexadecylpyridinium chloride (Sinopharm Chemical Reagent Co., Ltd, China) for 15 min at 37 °C. 100 μL elution from each well was transferred into a 96-well plate to detect the absorbance at 562 nm wavelength.

2.3.6. Real-time polymerase chain reaction (RT-PCR)

The relative osteogenic gene expression level of BMSCs cultured on 3D, 3DA and SLA surfaces was determined by RT-PCR after osteogenic inducing for 4, 7 and 10 days. The cell culturing and osteogenic inducing protocols were the same as the ALP activity assay. Total RNA was extracted using Trizol reagent (Takara Bio, Japan) at each timepoint and reversely transcribed to cDNA by a Prime-Script RT reagent kit (Takara Bio, Japan). cDNA samples were 1:10 diluted in RNase-free water before the PCR reaction. Primers used in the present study were synthesized commercially by Shengong Co., Ltd, China. Relative expression levels of osteogenic genes, such as RUNX2, OPN, BMP-2 and OCN were detected by a Light Cycler® 96 Real-Time PCR System (Roche, Switzerland) using a SYBR green PCR reaction mix (Takara Bio, Japan) according to the manufacturer's recommendation. β-actin was used as the reference in this study.

2.4. In vivo studies

2.4.1. Animal surgery procedure

The femoral condyle model was used to evaluate the *in vivo* osseointegration of 3D, 3DA and SLA implants. The animal experiments were approved by the Institutional Animal Care and Use Committee of Tongji University. Briefly, SD rats weighted approximately 280 g were given general anesthesia and the surgical site was shaved and disinfected. After exposing the implantation position, a hole was prepared and a sample were inserted. Finally, tissues were sutured in layers and all rats received antibiotics for 3 days to prevent infection. After 3 or 6 weeks of implantation, animals were euthanized by injecting overdose anesthetics and the femoral condyles were resected and fixed in 4% paraformaldehyde for histological analysis.

2.4.2. Histological and histomorphometric analysis

Samples were rinsed by flowing water and then dehydrated in ascending ethanol series from 50% to 100% sequentially before embedded in polymethyl methacrylate (PMMA) for undecalcified sectioning. The sectioning procedure was implemented by a diamond circular saw system (Exakt Apparatebau, Germany) and a grinding system (Exakt Apparatbau, Germany). The final sections were approximately 30 μm in thickness and were stained by van Gieson's picric fuchsin and observed by a light microscope (Nikon, Japan). For histomorphometric analysis, images captured by a digital camera were measured using Image-Pro Plus 6.0 software (Media Cybernetics Inc., USA) and bone-to-implant contact (BIC) percentages were calculated.

2.5. Statistical analysis

The data are presented as the mean $\pm$ one standard deviation (SD). All data were statistically analyzed by SPSS 22.0 software (SPSS Inc., USA). A one-way analysis of variance (ANOVA) was used to determine the level of significance accompanied by a Student–Newman–Keuls post hoc test. The difference was considered significant when the *P* value was < 0.05.

3. Results

3.1. Surface morphology and characteristics

The topography of 3D, 3DA and SLA surfaces was showed in Fig. 1. 3D surfaces remained the micron-scale 'hills and valleys' topographies with many partly-fused spherical particles interspersed on the solid fluctuant substrate, while lacking of submicron-scale structures (Fig. 1A and D). After acid etching, submicron-scale (2–5 μm) pits distributed uniformly on 3DA surfaces with the inherent micron-scale features of original 3D surfaces maintained (Fig. 1B and E). The SLA surface seemed in disarray with micron-scale concaved features obtained by sandblasting and similar submicron-scale pits produced by the same etching procedure as 3DA surfaces (Fig. 1C and F).

After acid etching, the average deviation of height (Sa) of 3D surfaces decreased from 19.18 ± 2.85 μm to 16.34 ± 0.97 μm (Fig. 2A) and root mean square height deviation (Sq) decreased from 25.52 ± 1.83 μm to 20.36 ± 1.02 μm (Fig. 2B). However, the 3DA surface was still significantly rougher than the SLA surface, the parameters of which were 7.69 ± 0.48 μm and 9.77 ± 0.51 μm, respectively. The developed surface ratio (Sdr) of 3DA surfaces (1.40 ± 0.11) declined by over 40% of the 3D surface (2.41 ± 0.20), while still significantly higher than that of the SLA surface (1.11 ± 0.11) (Fig. 2C). Furthermore, the contact angles of 3DA ($115° \pm 3°$) and SLA ($118° \pm 2°$) surfaces were comparable but significantly larger than that of the 3D group ($72° \pm 11°$) (Fig. 2D).

3.2. In vitro studies

3.2.1. Cell morphology and proliferation

The morphology of BMSCs adhered on 3D, 3DA and SLA surfaces after culturing for 24 h was observed by SEM (Fig. 3). Generally, cells acquired well-extended polygonal morphology on all three types of surfaces, whereas more pseudopods were observed on 3DA and SLA surfaces (Fig. 3B and C). As for cell number, there was no significant difference among three groups at day 1, but as the elongation of culturing time to days 4 and 7, the cell number increased more rapidly on 3DA and SLA surfaces with no significance between these two groups. With further increasing of the culturing time to 10 days, the difference among three groups diminished (Fig. 3D).

3.2.2. ALP activity and extracellular matrix (ECM) mineralization

At day 4, the ALP activity was low for all three groups and no significant difference was detected (Fig. 4A). As the osteogenic inducing lasted to 7 days, the 3DA group showed higher ALP activity compared with the 3D group, while the SLA group exhibited the highest activity. This tendency was maintained to day 10 (Fig. 4A). The ECM mineralization was determined by alizarin red staining accompanied by semiquantitative analysis (Fig. 4B). Obviously, mineralization could be observed on all three surfaces after 14 days of osteogenic inducing, and the 3DA and SLA surfaces presented apparently more mineralized nodules. The semiquantitative analysis further validated that the mineralization levels on the 3DA and SLA surfaces were significantly higher than that on 3D surfaces.
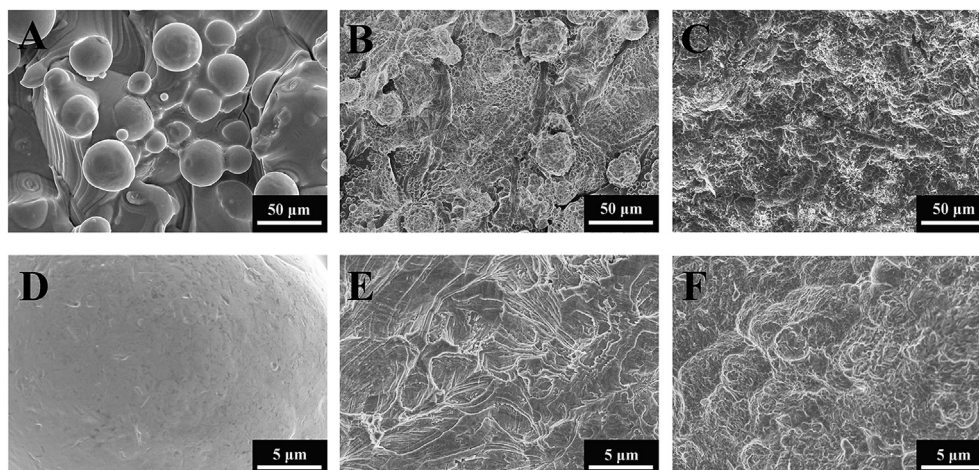

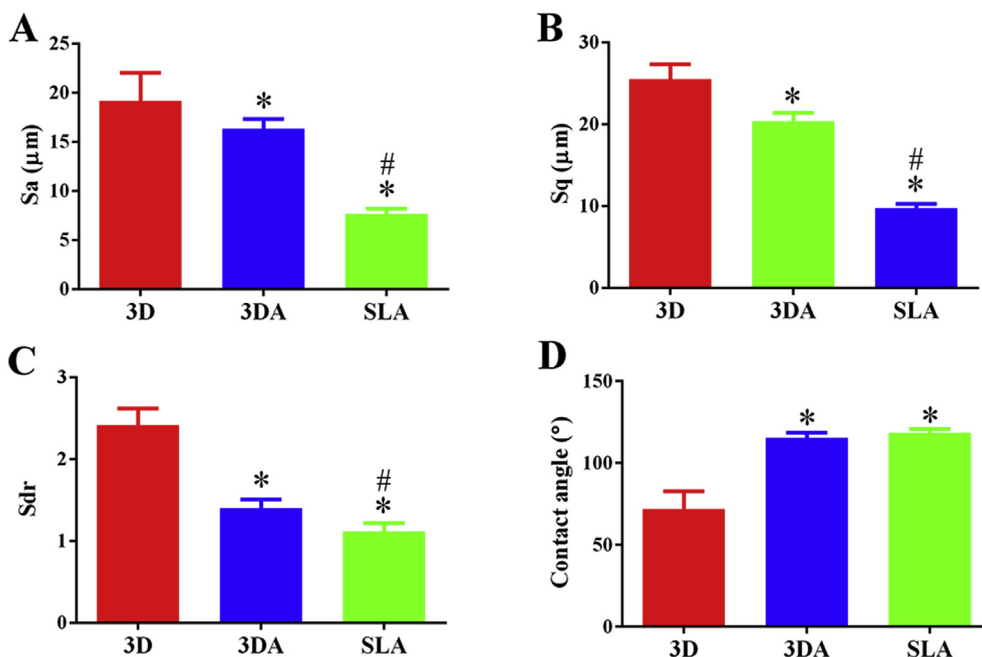**Fig. 1.** SEM micrographs of the 3D (A, D), 3DA (B, E) and SLA (C, F) surfaces.

Fig. 2. Surface characteristics of 3D, 3DA and SLA surfaces: (A–C) surface roughness parameters, (D) water contact angle; *$P < 0.05$ compared with the 3D group, #$P < 0.05$ compared with the 3DA group.

3.2.3. Relative expression levels of osteogenic genes

The osteogenic differentiation of BMSCs cultured on 3D, 3DA and SLA surfaces was further determined by detecting the relative expression level of osteogenic genes at mRNA level (Fig. 5). After 4 days of osteogenic inducing, the relative expression level of RUNX2, OPN, BMP-2 and OCN was comparable between the 3D and 3DA group, while significantly lower than that on the SLA surface except RUNX2. At day 7, the relative expression level of all markers except OPN on the 3DA surface was significantly higer than that on the 3D surface, though still lower than that on the SLA surface. This tendency between groups at day 7 was maintained to day 10, with the relative expression level of OPN becoming significantly higher than that on the 3D surface as well (Fig. 5).
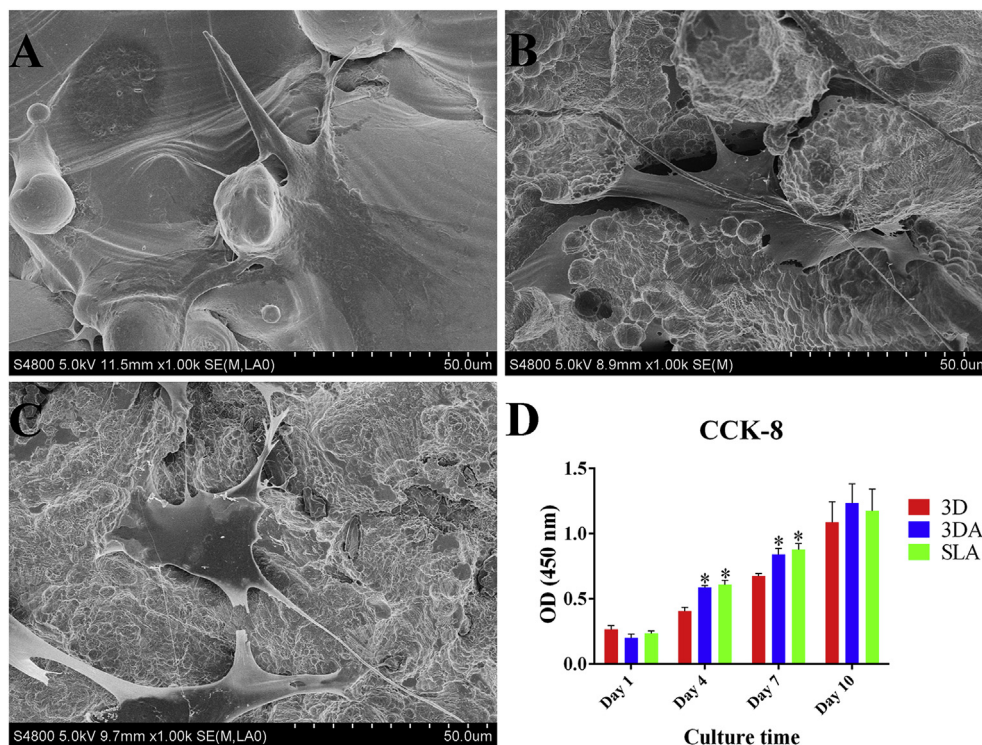

Fig. 3. Cell morphology on the 3D (A), 3DA (B) and SLA (C) surface after culturing of BMSCs for 24 h observed by SEM; (D) cell proliferation on surfaces assessed at days 1, 4, 7 and 10; *$P < 0.05$ compared with the 3D group.
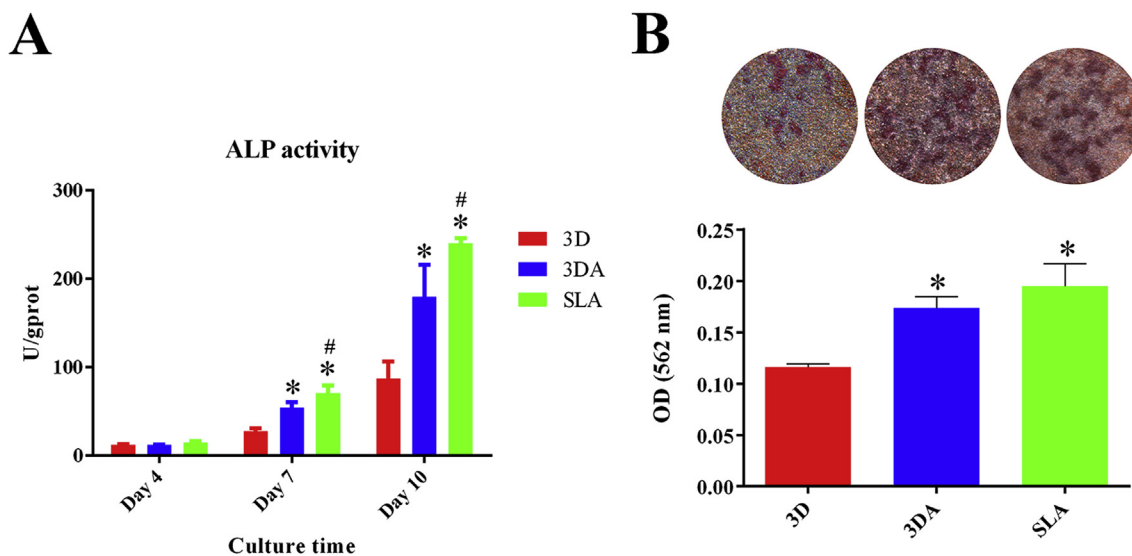
Fig. 4. (A) ALP activity of BMSCs cultured on 3D, 3DA and SLA surfaces after osteogenic inducing for 4, 7 and 10 days; (B) Representative images of ECM mineralization and semiquantitative analysis after osteogenic inducing for 14 days; *$P < 0.05$ compared with the 3D group, #$P < 0.05$ compared with the 3DA group.

3.3. In vivo studies

The *in vivo* osteointegration of 3D, 3DA and SLA implants was studied after implantation into the femoral condyle of SD rats for 3 and 6 weeks, respectively (Fig. 6). At week 3, there was very limited amount of bone that directly contacted with the 3D surface, compared with the 3DA and SLA surface. As the healing time extended to 6 weeks, the amount of contacted bone on implant surfaces obviously increased for all three groups. It was clear that the 3D group still remained the least amount while the SLA group increased most prominently (Fig. 6A).
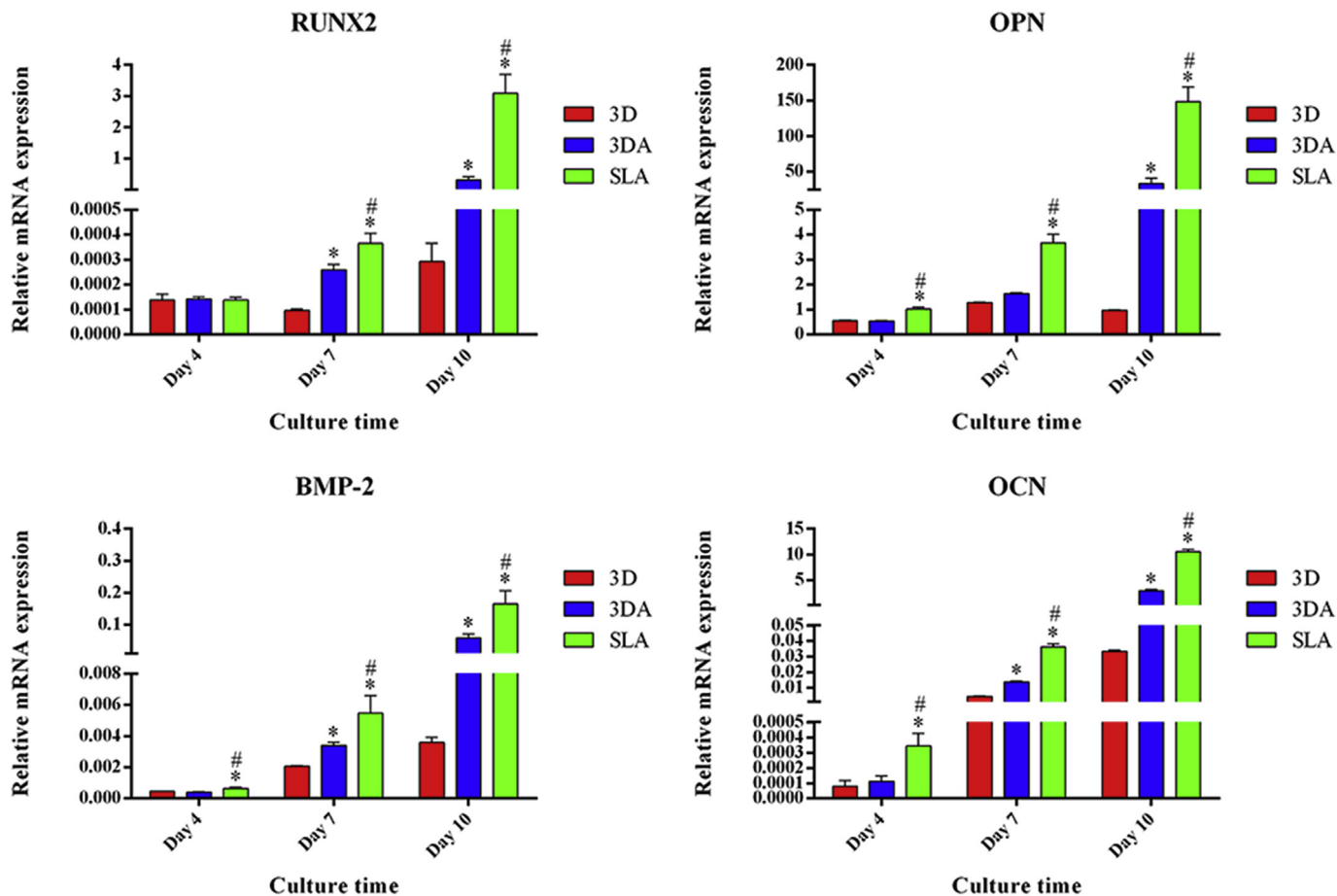

Fig. 5. Relative expression levels of osteogenic genes determined by RT-PCR after osteogenic inducing for 4, 7 and 10 days; *$P < 0.05$ compared with the 3D group, #$P < 0.05$ compared with the 3DA group.
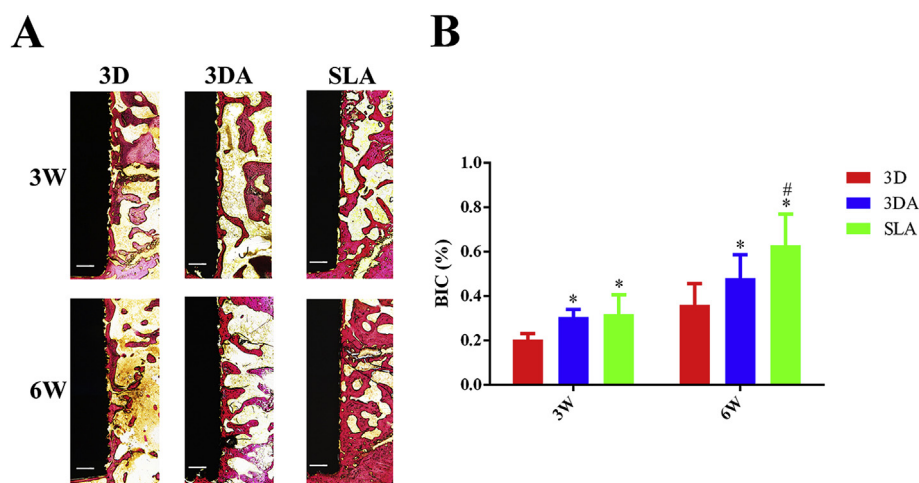
Fig. 6. Representative histological images of undecalcified sections of 3D, 3DA and SLA implants after implantation for 3 and 6 weeks, respectively (scale bar = 200 μm); (B) quantification of BIC percentages on implant surfaces; *$P < 0.05$ compared with the 3D group, #$P < 0.05$ compared with the 3DA group.

Accordingly, the quantitative data validated the average BIC percentage for the 3D group at week 3 was significantly lower than that of the 3DA and SLA groups and the percentage between 3DA and SLA group was comparable (Fig. 6B). However, when it came to week 6, the SLA group showed significantly higher BIC percentage than that of the 3DA group, though the 3DA surface had significant improvement compared with the 3D surface (Fig. 6B).

4. Discussion

Though it is controversial about what is the exact optimal surface design of implants, inspired by the structure of natural bone and implied by increasing number of researches, it is accepted that to construct hierarchical hybrid topological structures is the future direction of efforts [19,23,24]. The SLA surface is one of the most representative hierarchical titanium surfaces and has been proved by numerous literatures to be successful experimentally and clinically [20,21]. Clinical practice has confirmed that ITI® implants with the SLA surface could obtain a highly predictable success after implantation for as early as 6 weeks [25]. Since the 3D-printed titanium surface is inherent with micron-scale features, acid etching was utilized in the present study to create submicron-scale pits on the 3D surface, attempting to simulate the hierarchical micro/submicro-textured SLA surface. As showed in Fig. 1, hierarchical micro/submicro-textured 3DA and SLA surfaces were successfully constructed. Submicron-scale pits were embedded on the 3DA surface while maintaining the original micron-scale topographies (Fig. 1B and E). On the other hand, similar submicron-scale features were observed on the SLA surface (Fig. 1C and F), since they were simultaneously created through the same acid etching procedure.

Many literatures, researching the response of osteogenic cells to surface topographies, have employed substrates with complex hybrid architectures. Thus it is confusing that which topographical aspects of the surface are responsible for the ultimate biological effects, videlicet, whether there is a correspondence between specific architectural features and physiological responses. Zinger et al. [26] studied the response of osteoblasts to specific micron-scale and submicron-scale architectural features created by photolithography and acid etching, respectively. Their work suggested cell morphology, especially filopodia attachment, was correlated with the presence of submicron-scale pits, which evidently promoted osteogenic differentiation as well. Similar phenomena were observed in the present study. The observation of adhered cell morphology at 24 h suggested there was affluent pseudopods stretching outwardly from cells on the 3DA and SLA surfaces to interact with submicron-scale pits in contrast with the 3D group (Fig. 3A, B and C). And the osteogenic differentiation was significantly enhanced on the 3DA and SLA surfaces determined by the ALP activity, ECM mineralization, and the RT-PCR results (Figs. 4 and 5). Furthermore, many other previous reports also emphysized the stimulation effect of submicron-scale structures on biological responses of osteogenic cells [27,28].

However, it cannot be neglected there was an apparent gap of osteogenic differentiation between the 3DA and SLA groups (Figs. 4 and 5). This might be attributed to the difference of exact micron-scale features of 3DA and SLA surfaces (Fig. 1B and C) as they were produced by different processes. It has been reported that the geometry, three-dimensional size, distribution patterns (randomly or orderly) and other aspects of micron-scale features could differently alter cell functions [23,29]. The work of Zinger et al. [26] also indicated that the dimension and spacing of microcavities affected the attachment of osteoblasts and these were also important signals modulating osteoblast differentiation through regulating local factor production. Furthermore, the comparable ECM mineralization between SLA and 3DA surfaces (Fig. 4B) could be ascribed to the rougher and severer fluctuant surface features of 3DA surfaces (Figs. 1 and 2). It was assumed that 3DA surfaces could provide broader three-dimensional space than SLA surfaces, thus the duration of mineralization deposition would be longer. Therefore, there was timepoint at which the quantity of ECM mineralization on 3DA surfaces would catch or even surpass the SLA group.

Moreover, the general surface roughness has been demonstrated by many researches to be a crucial factor affecting the response of osteogenic cells. However, it is hard to draw a conclusion due to the diversity of material types, specific topographical features, surface characterizing methods to measure roughness parameters and so on. Faia-Torres et al. [30] studied the osteogenic differentiation of MSCs on surface roughness gradients and concluded that the moderate range of gradients, the average roughness (Ra) and mean distance between peaks (RSm) of which were around 2.1–3.1 μm and 71.1–48.1 μm respectively, obtained the best osteogenic performance. In the present study, surface roughness parameters of 3DA surfaces were generally lower than those of 3D surfaces after acid etching but still significantly higher than those of SLA surfaces (Fig. 2A, B and C), which might contribute to the discrepant osteogenic differentiation of BMSCs. Surface wettability is another critical factor that can affect physiological events during bone formation. It can be influenced by multiple other surface characteristics, such as surface energy, surface chemistry and surface topography, but the exact underlying mechanism is complicated [31,32]. In the present study, the contact angle on both hierarchical surfaces was apparently larger than that of the 3D group (Fig. 2D), which was consistent with some literatures suggesting acid etching procedure could decrease surface wettability [31,33].

Davies [34] expatiated the structure of *in vivo* bone-bonding interfaces and addressed that contact osteogenesis required a sufficiently stable surface consisting of micron-scale topography modified with submicron-scale undercuts, which could be recapitulated on implant surfaces. The present study just provided an evidence of this argument. The *in vivo* osseointegration of hierarchical micro/submicro-textured 3DA and SLA surfaces was obviously better than 3D surfaces (Fig. 6). This was consistent with our *in vitro* results: superior proliferation and differentiation of osteogenic cells are corelated with faster and larger volume of new bone formation *in vivo*. Meanwhile, there was an increasing gap of BIC percentage between 3DA and SLA surfaces during the implantation time extended from 3 weeks to 6 weeks (Fig. 6B). It is generally accepted that higher surface roughness is beneficial to the mechanical interlocking between implants and the around host bone, thus promoting the stability of implants [35,36]. Therefore, it is presumed that the better mechanical stability of 3DA implants, inspired by higher surface roughness, compensated the relatively insufficient of biolocial effect compared with the SLA group in the initial osseointegration stage. While as the healing time extended to 6 weeks, the superior osteogenic differentiation capacity of SLA surfaces dominated the osseointegration process and the gap of BIC percentages between 3DA and SLA groups increased to be significant (Fig. 6). It is accepted that nano-topography can promote osteogenic differentiation [37]. Titanium nanotubes (TNTs) are one of the most frequently reported nano-topographies in the field of titanium implant surface modification. In addition to the topographical cue, TNTs can also serve as a delivery system to storage and release bioactive molecules [38]. Therefore, TNTs can be employed to further improve the osteogenic performance of hierarchically modified 3D-printed Ti6Al4V implants in our subsequent study.

5. Conclusions

The hierarchical micro/submicro-textured 3D-printed surface was obtained by an acid etching procedure to enhance the osteogenic performance of 3D-printed Ti6Al4V implants. The adhered morphology, proliferation and osteogenic differentiation of BMSCs, as well as *in vivo* osseointegration on the hierarchically modified surface were significantly promoted. Though the specific submicron-scale topography was the same as SLA surfaces, 3DA surfaces were generally rougher, which could in turn provide better mechanical stability. However, the overall osteogenic performance of 3DA surfaces was not as good as the conventional SLA surface which has been applied clinically. Thus, further modification is desired before the clinical application of 3D-printed Ti6Al4V implants.

Credit author statement

The authors declare that this manuscript has not been published previously, and that it is not under consideration for publication elsewhere. All the authors have confirmed the submission of this manuscript.

Declaration of competing interest

The authors have no potential conflict of interests to disclose.

Acknowledgements

References

[1] J.R. Tumbleston, D. Shirvanyants, N. Ermoshkin, R. Janusziewicz, A.R. Johnson, D. Kelly, et al., Additive manufacturing. Continuous liquid interface production of 3D objects, Science 347 (2015) 1349–1352, https://doi.org/10.1126/science.aaa2397.

[2] Y. Li, S. Ding, C. Wen, Additive manufacturing technology for porous metal implant applications and triple minimal surface structures: a review, Bioact. Mater. 4 (2019) 56–70, https://doi.org/10.1016/j.bioactmat.2018.12.003.

[3] S. Derakhshanfar, R. Mbeleck, K. Xu, X. Zhang, W. Zhong, M. Xing, 3D bioprinting for biomedical devices and tissue engineering: a review of recent trends and advances, Bioact. Mater. 3 (2018) 144–156, https://doi.org/10.1016/j.bioactmat.2017.11.008.

[4] S. Dong, Y. Chen, L. Yu, K. Lin, X. Wang, Magnetic hyperthermia-synergistic H2O2 self-sufficient catalytic suppression of osteosarcoma with enhanced bone-regeneration bioactivity by 3D-printing composite scaffolds, Adv. Funct. Mater. (2019), https://doi.org/10.1002/adfm.201907071.

[5] T.K. Morimoto, J.D. Greer, E.W. Hawkes, M.H. Hsieh, A.M. Okamura, Toward the design of personalized continuum surgical robots, Ann. Biomed. Eng. 46 (2018) 1522–1533, https://doi.org/10.1007/s10439-018-2062-2.

[6] J. Koffler, W. Zhu, X. Qu, O. Platoshyn, J.N. Dulin, J. Brock, et al., Biomimetic 3D-printed scaffolds for spinal cord injury repair, Nat. Med. 25 (2019) 263–269, https://doi.org/10.1038/s41591-018-0296-z.

[7] S. Bose, D. Ke, H. Sahasrabudhe, A. Bandyopadhyay, Additive manufacturing of biomaterials, Prog. Mater. Sci. 93 (2018) 45–111, https://doi.org/10.1016/j.pmatsci.2017.08.003.

[8] J. Zhang, W. Zhou, H. Wang, K. Lin, F. Chen, 3D-printed surface promoting osteogenic differentiation and angiogenetic factor expression of BMSCs on Ti6Al4V implants and early osseointegration in vivo, J. Mater. Sci. Technol. 35 (2019) 336–343, https://doi.org/10.1016/j.jmst.2018.09.063.

[9] J.-a.N. Oliver, Y. Su, X. Lu, P.-H. Kuo, J. Du, D. Zhu, Bioactive glass coatings on metallic implants for biomedical applications, Bioact. Mater. 4 (2019) 261–270, https://doi.org/10.1016/j.bioactmat.2019.09.002.

[10] X. Ge, C. Ren, Y. Ding, G. Chen, X. Lu, K. Wang, et al., Micro/nano-structured TiO2 surface with dual-functional antibacterial effects for biomedical applications, Bioact. Mater. 4 (2019) 346–357, https://doi.org/10.1016/j.bioactmat.2019.10.006.

[11] H. Wang, C. Lin, X. Zhang, K. Lin, X. Wang, S.G. Shen, Mussel-inspired polydopamine coating: a general strategy to enhance osteogenic differentiation and osseointegration for diverse implants, ACS Appl. Mater. Interfaces 11 (2019) 7615–7625, https://doi.org/10.1021/acsami.8b21558.

[12] L. Xia, Y. Xie, B. Fang, X. Wang, K. Lin, In situ modulation of crystallinity and nano-structures to enhance the stability and osseointegration of hydroxyapatite coatings on Ti-6Al-4V implants, Chem. Eng. J. 347 (2018) 711–720, https://doi.org/10.1016/j.cej.2018.04.045.

[13] X. Zhang, H. Li, J. Liu, H. Wang, W. Sun, K. Lin, et al., Amorphous carbon modification on implant surface: a general strategy to enhance osteogenic differentiation for diverse biomaterials via FAK/ERK1/2 signaling pathways, J. Mater. Chem. B. 7 (2019) 2518–2533, https://doi.org/10.1039/c8tb02850h.

[14] G. Mendonca, D.B.S. Mendonca, F.J.L. Aragao, L.F. Cooper, Advancing dental implant surface technology - from micron- to nanotopography, Biomaterials 29 (2008) 3822–3835, https://doi.org/10.1016/j.biomaterials.2008.05.012.

[15] X. Zhang, H. Li, C. Lin, C. Ning, K. Lin, Synergetic topography and chemistry cues guiding osteogenic differentiation in bone marrow stromal cells through ERK1/2 and p38 MAPK signaling pathway, Biomater. Sci. 6 (2018) 418–430, https://doi.org/10.1039/c7bm01044c.

[16] S. Dong, X. Wang, G.S. Shen, X. Wang, K. Lin, Research progress on functional modifications and applications of bioceramic scaffolds, J. Inorg. Mater. (2019), https://doi.org/10.15541/jim20190561.

[17] A. Rodriguez-Contreras, D.G. Bello, A. Nanci, Surface nanoporosity has a greater influence on osteogenic and bacterial cell adhesion than crystallinity and wettability, Appl. Surf. Sci. 445 (2018) 255–261, https://doi.org/10.1016/j.apsusc.2018.03.150.

[18] J.Y. Rho, L. Kuhn-Spearing, P. Zioupos, Mechanical properties and the hierarchical structure of bone, Med. Eng. Phys. 20 (1998) 92–102, https://doi.org/10.1016/s1350-4533(98)00007-1.

[19] F.A. Shah, P. Thomsen, A. Palmquist, Osseointegration and current interpretations of the bone-implant interface, Acta Biomater. 84 (2019) 1–15, https://doi.org/10.1016/j.actbio.2018.11.018.

[20] G. Zhao, A.L. Raines, M. Wieland, Z. Schwartz, B.D. Boyan, Requirement for both micron and submicron scale structure for synergistic responses of osteoblasts to substrate surface energy and topography, Biomaterials 28 (2007) 2821–2829, https://doi.org/10.1016/j.biomaterials.2007.02.024.

[21] D. Buser, S.F. Janner, J.G. Wittneben, U. Brägger, C.A. Ramseier, G.E. Salvi, 10-year survival and success rates of 511 titanium implants with a sandblasted and acid-etched surface: a retrospective study in 303 partially edentulous patients, Clin. Implant Dent. Relat. Res. 14 (2012) 839–851, https://doi.org/10.1111/j.1708-8208.2012.00456.x.

[22] Y. Zhu, H. Cao, S. Qiao, M. Wang, Y. Gu, H. Luo, et al., Hierarchical micro/nanostructured titanium with balanced actions to bacterial and mammalian cells for dental implants, Int. J. Nanomed. 10 (2015) 6659–6674, https://doi.org/10.2147/

IJN.S92110.

[23] M. Nikkhah, F. Edalat, S. Manoucheri, A. Khademhosseini, Engineering microscale topographies to control the cell-substrate interface, Biomaterials 33 (2012) 5230–5246, https://doi.org/10.1016/j.biomaterials.2012.03.079.

[24] E.G. Long, M. Buluk, M.B. Gallagher, J.M. Schneider, J.L. Brown, Human mesenchymal stem cell morphology, migration, and differentiation on micro and nanotextured titanium, Bioact. Mater. 4 (2019) 249–255, https://doi.org/10.1016/j.bioactmat.2019.08.001.

[25] D.L. Cochran, D. Buser, C.M. ten Bruggenkate, D. Weingart, T.M. Taylor, J.P. Bernard, et al., The use of reduced healing times on ITI (R) implants with a sandblasted and acid-etched (SLA) surface: early results from clinical trials on ITI (R) SLA implants, Clin. Oral Implant. Res. 13 (2002) 144–153, https://doi.org/10.1034/j.1600-0501.2002.130204.x.

[26] O. Zinger, G. Zhao, Z. Schwartz, J. Simpson, M. Wieland, D. Landolt, et al., Differential regulation of osteoblasts by substrate microstructural features, Biomaterials 26 (2005) 1837–1847, https://doi.org/10.1016/j.biomaterials.2004.06.035.

[27] G. Zhao, O. Zinger, Z. Schwartz, M. Wieland, D. Landolt, B.D. Boyan, Osteoblast-like cells are sensitive to submicron-scale surface structure, Clin. Oral Implant. Res. 17 (2006) 258–264, https://doi.org/10.1111/j.1600-0501.2005.01195.x https://search.crossref.org/?q=Osteoblast-like+cells+are+sensitive+to+submicron-scale+surface+structure.

[28] M.O. Klein, A. Bijelic, T. Toyoshima, H. Götz, R.L. Von Koppenfels, B. Al-Nawas, et al., Long-term response of osteogenic cells on micron and submicron-scale-structured hydrophilic titanium surfaces: sequence of cell proliferation and cell differentiation, Clin. Oral Implant. Res. 21 (2010) 642–649, https://doi.org/10.1111/j.1600-0501.2009.01883.x.

[29] J. Fu, Y.Y. Hu, Z. Guo, Y.Q. Zhang, Y.L. Hao, S.J. Li, Effect of surface micro-topography of titanium material on the behaviors of rabbit osteoblast in vitro, Appl. Surf. Sci. 255 (2008) 286–289, https://doi.org/10.1016/j.apsusc.2008.06.064.

[30] A.B. Faia-Torres, S. Guimond-Lischer, M. Rottmar, M. Charnley, T. Goren, K. Maniura-Weber, et al., Differential regulation of osteogenic differentiation of stem cells on surface roughness gradients, Biomaterials 35 (2014) 9023–9032, https://doi.org/10.1016/j.biomaterials.2014.07.015.

[31] F. Rupp, R.A. Gittens, L. Scheideler, A. Marmur, B.D. Boyan, Z. Schwartz, et al., A review on the wettability of dental implant surfaces I: theoretical and experimental aspects, Acta Biomater. 10 (2014) 2894–2906, https://doi.org/10.1016/j.actbio.2014.02.040.

[32] Z.-Y. Shi, Q. Li, S.-C. Tang, J. Qian, Y.-K. Pan, J. Wei, Surface modification on property of mesoporous calcium magnesium silicate/polyetheretherketone composites, J. Inorg. Mater. 33 (2018) 67–74, https://doi.org/10.15541/jim20170120.

[33] R. Kobatake, K. Doi, Y. Oki, H. Umehara, H. Kawano, T. Kubo, et al., Investigation of effective modification treatments for titanium membranes, Appl. Sci.-Basel. 7 (2017), https://doi.org/10.3390/app7101022.

[34] J.E. Davies, Bone bonding at natural and biomaterial surfaces, Biomaterials 28 (2007) 5058–5067, https://doi.org/10.1016/j.biomaterials.2007.07.049.

[35] A. Tabassum, G.J. Meijer, J.G.C. Wolke, J.A. Jansen, Influence of surgical technique and surface roughness on the primary stability of an implant in artificial bone with different cortical thickness: a laboratory study, Clin. Oral Implant. Res. 21 (2010) 213–220, https://doi.org/10.1111/j.1600-0501.2009.01823.x.

[36] R. Agarwal, A.J. Garcia, Biomaterial strategies for engineering implants for enhanced osseointegration and bone repair, Adv. Drug Deliv. Rev. 94 (2015) 53–62, https://doi.org/10.1016/j.addr.2015.03.013.

[37] K. Lin, L. Xia, J. Gan, Z. Zhang, H. Chen, X. Jiang, et al., Tailoring the nanostructured surfaces of hydroxyapatite bioceramics to promote protein adsorption, osteoblast growth, and osteogenic differentiation, ACS Appl. Mater. Interfaces 5 (2013) 8008–8017, https://doi.org/10.1021/am402089w.

[38] J. Chen, X. Shi, Y. Zhu, Y. Chen, M. Gao, H. Gao, et al., On-demand storage and release of antimicrobial peptides using Pandora's box-like nanotubes gated with a bacterial infection-responsive polymer, Theranostics 10 (2020) 109–122, https://doi.org/10.7150/thno.38388.